Differential Wheel Speed Sensor Integration with GPS/INS for Land Vehicle Navigation

Andrew C. Hazlett,* John L. Crassidis,† Daniel P. Fuglewicz‡
University at Buffalo, The State University of New York, Buffalo, NY 14260

Patrick Miller§
Calspan Corporation, Buffalo, NY 14225

This paper develops an approach for the integration of GPS, inertial measurements from accelerometers and gyros, and differential wheel speed sensors for land vehicle navigation. Incorporating differential wheel speed sensor information into land vehicle navigation provides a solution for eliminating large errors caused by vehicle motions while also reducing errors from sideslip. Extended Kalman and Unscented filtering algorithms are designed with a six degree of freedom model. In order to incorporate differential wheel speed information properly, the effective wheel radius must also be estimated as part of the overall estimation approach. Simulation results show the performance of the filters for cases of GPS/INS with and without the wheel speed sensor.

I. Introduction

The Global Positioning System (GPS) combined with an Inertial Navigation System (INS) has been extensively executed for position determination in vehicle navigation.[1] GPS alone, with the use of a single receiver, can be used to find absolute position up to within a radius of 10 meters.[2] Alternate variations, such as Differential GPS (DGPS), which uses a fixed base station, and the Wide Area Augmentation System (WAAS) may allow the position to be found within a meter.[3] Even with this high level of precision, a land vehicle cannot use a GPS receiver alone to continuously find position. To compute position using a GPS receiver a signal from at least four satellites must be available for long enough to receive the encoded information.[4] This transmitted signal is at a frequency of 1.575 GHz, which is too high to pass through or bend around obstacles such as dense foliage, rugged terrain, tunnels, under bridges or in an urban environment with tall buildings. Due to these obstacles, additional navigation aids are required for most land vehicle navigation applications. Exceptions to this exist for certain land vehicle applications such as autonomous farm vehicles[5] because satellite signals are not impeded in open fields. As of this writing a GPS receiver costs between $50 and $500 depending on the measurement update rate, which is typically between 1 to 10 Hz.[3]

Navigation with sensors that do not measure absolute position of a vehicle is collectively referred to as dead-reckoning.[4] Because dead-reckoning sensors do not measure an absolute position they have errors from sensor drift that grow without bound if not used in conjunction with an absolute position measurement. An example of a dead-reckoning sensor is an INS consisting of gyros and accelerometers. In this paper another dead-reckoning sensor involving differential wheel speed measurements is considered for land navigation. The use of dead-reckoning may be described as a flywheel to keep accurate position measurements for short term GPS outages and to smooth the low update rate of GPS. Over long periods of time GPS is required to

*Student, Aerospace Engineering, Email: ahazlett@buffalo.edu, Student Member AIAA.
†Professor, Department of Mechanical and Aerospace Engineering, Email: johnc@buffalo.edu, Associate Fellow AIAA.
‡Senior Engineering Manager, Experimental Campus for Large Infrastructure Protection, Sustainability, and Enhancement (ECLIPSE), Multidisciplinary Center for Earthquake Engineering (MCEER), Department of Civil, Structural and Environmental Engineering, Email: dpf@buffalo.edu.
§Senior Engineer, Systems Engineering Group, 4455 Genesee Street, Email: patrick.miller@calspan.com.

calibrate the dead-reckoning sensor drift. The fusion of GPS and dead-reckoning sensors counter limitations that exist in each, creating an advantage to using them in conjunction.

With the advent of less expensive INS sensors, especially Micro-Electrical Mechanical Systems (MEMS), it is now a reality to use these sensors for land vehicle navigation applications. These less expensive sensors do not perform as well as high-accuracy sensors in terms of drift and white-noise measurement errors, but are compensated for when combined with GPS.[6] The INS sensors considered in the present research include accelerometers and rate gyroscopes. Currently inexpensive MEMS accelerometers and gyros cost less than $30, with update rates on the order of 100 Hz.[3]

The rear wheel speed sensors incorporated into the present research provides measurements of the vehicle's yaw rate and the velocity in the vehicle's heading direction. Wheel speed sensors currently exist as part of an Anti-lock Brake System (ABS), which is a standard feature on many present day land vehicles.[7] The wheel speed sensor integration into navigation systems to find position has been studied by Kubo and Gao.[8,9] In this previous work two conditions must be met in order for the integration of the wheel speed sensor to produce valid results; the vehicle must operate on a flat road and no side slip may occur.[9] These conditions do not always hold, such as the large side slip that exists when a vehicle travels on a bumpy surface or off-road. Note that side-slip is also a function of yaw rate, speed, and vehicle weight distribution. Side slip occurs instantaneously, and is not easily modeled. Much research has been conducted into creating approximations for modeling side slip.[5,10] Another method used to avoid the errors caused by side slip is to detect it and use an adaptive estimation algorithm that bypasses the wheel speed measurement when an unacceptable level occurs. An additional error source is created from pressure variations in the tire. This may be accounted for by including each wheel radius as a state variable. Without this, large errors occur when the rear wheel radii vary, such as the case of using a spare tire where the wheel radius may change over 5 cm.[11]

In navigation the most common method of integrating GPS and INS has been with an Extended Kalman Filter (EKF).[12] A well-known drawback of the EKF is that if the errors are not within the linear region, the filter may diverge. This is especially relevant with GPS/INS integration due to unknown attitude and inertial sensor calibration parameters *a priori*. One aspect of the EKF algorithm design is the method of how a measurement is processed, which may be categorized in two categories; loosely or tightly coupled.[6] Tightly coupled refers to when the measurement is directly used in the filter as it is provided by the sensor. Loosely coupled uses an estimated value of a current state in the filter that is found from the sensor output. The loose-tight coupling distinction is independent for each measurement used in the filter. As for a GPS sensor a tightly coupled configuration allows for position information to be provided with a minimum of only three satellite signals but also requires knowledge of variables used in the tracking loops that may not be readily available.[6] In the present research the GPS measurement is integrated into the EKF using a loosely coupled approach, in which a minimum of four GPS satellite signals must be available. This requires independent position estimates from GPS to be used in the EKF as measurements. Alternately, the differential wheel speed sensor measurements are used in a tightly coupled manner. This allows for no pre-processing of the measurements from the wheel speed sensors to be preformed and has been proven an effective approach by Carlson.[11]

In addition to the EKF an Unscented Filter (UF) is considered in the present research. The UF essentially provides derivative-free higher-order approximations by approximating a Gaussian distribution rather than approximating an arbitrary nonlinear function as in the EKF.[13] This provides several advantages over the EKF; a lower expected error, use on non-differentiable functions, no Jacobian matrix calculation and validity for higher order expansions.[6]

The organization of this paper is as follows. The various coordinate frames used in INS including transformations between frames are discussed in Section II. Section III provides the background for the attitude kinematics used in the estimation algorithm. The linearized equations are shown for the INS equations along with the measurement models for the inertial sensors in Section IV. The differential wheel speed sensor measurement model is defined in Section V. Section VI summarizes the states, measurements and linearized equations used to propagate the states in the filters. The EKF and UF algorithms are then defined in Sections VII and VIII. This leads to the simulation results and discussion of initial condition errors in Section IX.

II. Reference Frames

A. Earth-Centered-Inertial (ECI) Frame

The ECI frame is denoted by $\{\hat{\mathbf{i}}_1, \hat{\mathbf{i}}_2, \hat{\mathbf{i}}_3\}$ and the vectors described in this frame have superscript I (e.g., $\mathbf{r}^I$.) For the purpose of Earth based navigation this frame is considered inertial. This frame does not rotate with respect to the stars and has an origin at the center of Earth. The $\hat{\mathbf{i}}_3$ axis is aligned in the direction of Earth's North pole, the $\hat{\mathbf{i}}_1$ axis is aligned in the vernal equinox direction and the $\hat{\mathbf{i}}_2$ axis completes the right handed system.

B. Earth-Centered-Earth-Fixed (ECEF) Frame

The ECEF frame is denoted by $\{\hat{\mathbf{e}}_1, \hat{\mathbf{e}}_2, \hat{\mathbf{e}}_3\}$ and vectors described in this frame have superscript E (e.g., $\mathbf{r}^E$.) The ECEF frame has an origin at the center of Earth and is fixed to the Earth's motion, rotating with the Earth. For this frame $\hat{\mathbf{e}}_3 = \hat{\mathbf{i}}_3$, $\hat{\mathbf{e}}_1$ is in the direction of Earth's prime meridian and $\hat{\mathbf{e}}_2$ completes the right handed system. In this frame the $\hat{\mathbf{e}}_1$ and $\hat{\mathbf{e}}_2$ axes are rotated by Θ from the ECI frame.

C. Transformation From ECI to ECEF

The transformation between the ECI and ECEF frame involves only a single-axis rotation about $\hat{\mathbf{i}}_3$. This is defined by

$$\begin{bmatrix} x \\ y \\ z \end{bmatrix}^E = \begin{bmatrix} \cos\Theta & \sin\Theta & 0 \\ -\sin\Theta & \cos\Theta & 0 \\ 0 & 0 & 1 \end{bmatrix} \begin{bmatrix} x \\ y \\ z \end{bmatrix}^I \tag{1}$$

The angle Θ defines this transformation and can be found using the sidereal day. The solar The conversion from Universal Time Coordinated (UTC) to Greenwhich Mean Sidereal Time (GMST) is given by Meeus.[14]

D. Local North-East-Down (NED) Frame

The NED frame is denoted by $\{\hat{\mathbf{n}}, \hat{\mathbf{e}}, \hat{\mathbf{d}}\}$ and vectors described in this frame have the superscript N (e.g., $\mathbf{r}^N$.) This frame is used for local navigation due to the frame having an origin at the geodetic point of interest and the frame forming a plane normal to the surface of the Earth. The $\hat{\mathbf{d}}$ axis points to the center of the Earth, the $\hat{\mathbf{n}}$ axis points in the true North direction on Earth's surface and $\hat{\mathbf{e}}$ axis points true East on Earth's surface. This coordinate system also has the advantage of allowing the acceleration due to the Earth's gravity to be entirely in the $\hat{\mathbf{d}}$ direction.

E. Transformation From ECEF to NED

This transformation can be described as the combination of first a rotation from the ECEF frame to an East-North-Up (ENU) frame using latitude (λ) and longitude (Φ), and then a simple change in axes from the ENU to NED frames. This change in axes is described by $\hat{\mathbf{n}}^N = \hat{\mathbf{e}}^{ENU}$, $\hat{\mathbf{e}}^N = \hat{\mathbf{n}}^{ENU}$ and $\hat{\mathbf{d}}^N = -\hat{\mathbf{u}}^{ENU}$, allowing for a right hand system with the third component in the down direction. This rotation from ECEF to NED can be described with

$$A_E^N = \begin{bmatrix} -\sin\lambda\cos\Phi & -\sin\lambda\sin\Phi & \cos\lambda \\ -\sin\Phi & \cos\Phi & 0 \\ -\cos\lambda\cos\Phi & -\cos\lambda\sin\Phi & -\sin\lambda \end{bmatrix} \tag{2}$$

F. Body Frame

The body frame is denoted by $\{\hat{\mathbf{b}}_1, \hat{\mathbf{b}}_2, \hat{\mathbf{b}}_3\}$ and is described by the superscript B (e.g., $\mathbf{r}^B$.) This frame is fixed to and rotating with the body of interest.

G. Transformation From NED to Body

This last transformation is found from a 3-2-1 Euler angle rotation from the body to the NED frame. This rotation is defined by ϕ, θ and ψ, which are roll, pitch, and yaw, respectively. The following equation defines this relationship, showing the attitude matrix from the body-frame to the NED frame:

$$A_B^N = \begin{bmatrix} \cos\theta\cos\psi & -\cos\phi\sin\psi + \sin\phi\sin\theta\cos\psi & \sin\phi\sin\psi + \cos\phi\sin\theta\cos\psi \\ \cos\theta\sin\psi & \cos\psi\cos\phi + \sin\phi\sin\theta\sin\psi & -\sin\phi\cos\psi + \cos\phi\sin\theta\sin\psi \\ -\sin\theta & \sin\phi\cos\theta & \cos\phi\cos\theta \end{bmatrix} \tag{3}$$

H. Geodetic Coordinate System (LLH)

Geodetic coordinates are the navigational coordinate system used by GPS to navigate on the surface of Earth. Geodetic coordinates consist of latitude, longitude, and height (LLH), denoted as $\{\lambda, \Phi, h\}$. Latitude is the angle from the equator to the position of interest on Earth. Longitude is the angle measured from the prime meridian around the Earth to the location. The height represents the difference from the Earth's ellipsoid to the location, which is also known as altitude. This ellipsoid is approximated in the World Geodetic System 1984 (WGS-84) model.[15] Pertinent parameters for this model are shown in Table 1. These parameters are used in the transformation of coordinate frames from ECEF to LLH and back. This transformation is between different types of coordinate systems and thus has increased complexity from the attitude matrices that give the other coordinate transformations in this section. The transformation from LLH to ECEF is much simpler than the transformation from ECEF to LLH.

Table 1. WGS-84 Model Parameters

Parameter	Value	Description
a	6378137.0 m	Earth ellipsoid semi-major axis
b	63563124.2 m	Earth ellipsoid semi-minor axis
e	0.0818	Earth eccentricity
ω_e	7.292115×10^{-5} rad/sec	Earth rotation rate

I. Transformation From LLH to ECEF

The conversion from LLH to ECEF coordinates begins with the calculation of N, the length vector from the center of Earth's ellipsoid to the surface:[12]

$$N = \frac{a}{\sqrt{1 - e^2\sin^2\lambda}} \tag{4}$$

The ECEF coordinates can now be directly calculated using the following equations and the parameters from Table 1:

$$x = (N + h)\cos\lambda\cos\Phi \tag{5a}$$

$$y = (N + h)\cos\lambda\sin\Phi \tag{5b}$$

$$z = [N(1 - e^2) + h]\sin\lambda \tag{5c}$$

J. Transformation From ECEF to LLH

The conversion back to LLH is more complicated and is shown in the closed form solution from Zhu[16] using the parameters of Table 1:

$$w = \sqrt{x^2 + y^2}, \qquad l = \frac{e^2}{2}, \qquad m = (\frac{w}{a})^2 \tag{6a}$$

$$n = [(1 - e^2)z/b]^2, \qquad i = -(2l^2 + m + n)/2, \qquad k = l^2(l^2 - m - n) \tag{6b}$$

$$q = (m + n - 4l^2)^3/216 + mnl^2, \qquad D = \sqrt{(2q - mnl^2)mnl^2} \tag{6c}$$

$$\beta = i/3 - \sqrt[3]{q + D} - \sqrt[3]{q - D} \tag{6d}$$

$$t = \sqrt{\sqrt{\beta^2 - k} - (\beta + i)/2} - \text{sign}(m - n)\sqrt{(\beta - i)/2} \tag{6e}$$

$$w_1 = w/(t + l), \qquad z_1 = (1 - e^2)z/(t - l) \tag{6f}$$

$$\phi = \text{atan}(z_1/((1 - e^2)w_1)) \tag{6g}$$

$$\lambda = 2\text{atan}[(w - x)/y] \tag{6h}$$

$$h = \text{sign}(t - 1 + l)\sqrt{(w - w_1)^2 + (z - z_1)^2} \tag{6i}$$

For completeness, for the special case of being located at one of the Earth's poles, i.e. when $w = 0$, the height and latitude must be calculated as follows:

$$h = \text{sign}(z)z - b, \qquad \phi = \text{sign}(z)\pi/2 \tag{7}$$

III. Attitude Kinematics

This section summarizes the attitude kinematics that are used in the filter design. The attitude matrix consists of (3×3) dependent components that map the rotation from one frame to another. The attitude matrix can be parameterized using a smaller set of elements to represent the matrix. Methods of parameterizations include Euler axis/angle rotations, Euler angles, quaternions, and the Gibbs vector. The parameterization chosen is problem dependent based which method is most advantageous. Each of the parameterizations are equivalent and may be converted between one another.[17]

In this paper the quaternion is used extensively in the filter design due to the advantage of the existence of no singularities, no transcendental functions, and because successive rotations may be taken by quaternion multiplication. The attitude parameterization of the quaternion uses a four-dimensional vector which must satisfy the constraint $\mathbf{q}^T\mathbf{q} = 1$. The quaternion is defined as $\mathbf{q} = [\boldsymbol{\varrho}^T \;\; q_4]^T$, where $\boldsymbol{\varrho} = [q_1 \;\; q_2 \;\; q_3]^T$. The attitude matrix is related to the quaternion by the following equation:

$$A(\mathbf{q}) = \Xi^T(\mathbf{q})\Psi(\mathbf{q}) \tag{8}$$

in which

$$\Xi(\mathbf{q}) \equiv \begin{bmatrix} q_4 I_{4\times 4} + [\boldsymbol{\varrho}\times] \\ -\boldsymbol{\varrho}^T \end{bmatrix}, \quad \Psi(\mathbf{q}) \equiv \begin{bmatrix} q_4 I_{4\times 4} - [\boldsymbol{\varrho}\times] \\ -\boldsymbol{\varrho}^T \end{bmatrix} \tag{9}$$

The cross product matrix, $[\boldsymbol{\varrho}\times]$, is an operator defined as

$$[\boldsymbol{\varrho}\times] = \begin{bmatrix} 0 & -q_3 & q_2 \\ q_3 & 0 & -q_1 \\ -q_2 & q_1 & 0 \end{bmatrix} \tag{10}$$

The attitude kinematics equation for the body to NED frame is given by

$$\dot{A}_B^N = -[\boldsymbol{\omega}_{B/N}^B\times]A_N^B \tag{11}$$

The attitude kinematics equation for the NED to body frame is given by

$$\dot{A}_N^B = A_B^N[\boldsymbol{\omega}_{B/N}^B\times] \tag{12}$$

which is used to find the INS equations. From this, the quaternion kinematic relationship is given as

$$\dot{\mathbf{q}} = \frac{1}{2}\Xi(\mathbf{q})\boldsymbol{\omega}_{B/N}^B = \frac{1}{2}\Omega(\boldsymbol{\omega}_{B/N}^B)\mathbf{q} \tag{13}$$

with

$$\Omega(\omega_{B/N}^B) \equiv \begin{bmatrix} -[\boldsymbol{\omega}_{B/N}^B\times] & \boldsymbol{\omega}_{B/N}^B \\ -(\boldsymbol{\omega}_{B/N}^B)^T & 0 \end{bmatrix} \tag{14}$$

Additionally the inverse quaternion is defined as

$$\mathbf{q}^{-1} \equiv \begin{bmatrix} -\boldsymbol{\varrho} \\ q_4 \end{bmatrix} \tag{15}$$

IV. INS Equations

The inertial navigation equations used to propagate the states in the filters are defined in the NED coordinate system and include the quaternion parameterization:

$$\dot{\mathbf{q}} = \frac{1}{2}\Xi(\mathbf{q})\boldsymbol{\omega}^B_{B/N} \tag{16a}$$

$$\dot{\lambda} = \frac{v_N}{R_\lambda + h} \tag{16b}$$

$$\dot{\Phi} = \frac{v_E}{(R_\Phi + h)\cos\lambda} \tag{16c}$$

$$\dot{h} = -v_D \tag{16d}$$

$$\dot{v}_N = -\big[\frac{v_E}{(R_\Phi + h)\cos\lambda} + 2\omega_e\big]v_E \sin\lambda + \frac{v_N v_D}{R_\lambda + h} + a_N \tag{16e}$$

$$\dot{v}_E = -\big[\frac{v_E}{(R_\Phi + h)\cos\lambda} + 2\omega_e\big]v_N \sin\lambda + \frac{v_E v_D}{R_\Phi + h} + 2\omega_e v_D \cos\lambda + a_E \tag{16f}$$

$$\dot{v}_D = -\frac{v_E^2}{R_\Phi + h} - \frac{v_N^2}{R_\lambda + h} - 2\omega_e v_E \cos\lambda + g + a_D \tag{16g}$$

The following equations define the Earth's surface based on the latitude and longitude:

$$R_\lambda = \frac{a(1-e^2)}{(1 - e^2\sin^2\lambda)^{3/2}} \tag{17a}$$

$$R_\Phi = \frac{a}{(1 - e^2\sin^2\lambda)^{1/2}} \tag{17b}$$

The local gravity can be calculated as

$$\begin{aligned} g = {} & 9.780327(1 + 5.3924\times10^{-3}\sin^2\lambda - 5.8\times10^{-6}\sin^2 2\lambda) \\ & - (3.0877\times10^{-6} - 4.4\times10^{-9}\sin^2\lambda)h + 7.2\times10^{-14}h^2 \end{aligned} \tag{18}$$

The inertial measurements used in this paper come from a 3-axis rate gyroscope and a 3-axis accelerometer. When modeling both of these sensors a bias drift and white noise must be included to accurately depict the sensor properties. The measurement model for the rate gyroscope is given by

$$\tilde{\boldsymbol{\omega}}^B_{B/I} = \boldsymbol{\omega}^B_{B/I} + \mathbf{b}_g + \boldsymbol{\eta}_{gv} \tag{19}$$

$$\dot{\mathbf{b}}_g = \boldsymbol{\eta}_{gu} \tag{20}$$

where $\mathbf{b}_g$ is the gyroscope bias, and $\boldsymbol{\eta}_{gu}$ and $\boldsymbol{\eta}_{gv}$ are zero-mean Gaussian white-noise processes with spectral densities respectively given by $\sigma^2_{gu}I_{3\times3}$ and $\sigma^2_{gv}I_{3\times3}$. The measurement model for the accelerometer in body coordinates is given as follows:

$$\tilde{\mathbf{a}}^B = \mathbf{a}^B + \mathbf{b}_a + \boldsymbol{\eta}_{av} \tag{21}$$

$$\dot{\mathbf{b}}_a = \boldsymbol{\eta}_{au} \tag{22}$$

where $\mathbf{b}_a$ is the accelerometer bias, and $\boldsymbol{\eta}_{au}$ and $\boldsymbol{\eta}_{av}$ are zero-mean Gaussian white-noise processes with spectral densities respectively given by $\sigma^2_{au}I_{3\times3}$ and $\sigma^2_{av}I_{3\times3}$.

The measurement taken by the gyroscope cannot be directly used in the INS equations but can be converted from the ECI frame to the NED using

$$\boldsymbol{\omega}^B_{B/I} = \boldsymbol{\omega}^B_{B/N} + \boldsymbol{\omega}^B_{N/I} \tag{23}$$

where $\boldsymbol{\omega}^B_{B/N}$ can be found from

$$\boldsymbol{\omega}^B_{N/I} = A^B_N(\mathbf{q})\boldsymbol{\omega}^N_{N/I} \tag{24}$$

and $\boldsymbol{\omega}_{N/I}^N$ is defined as

$$\boldsymbol{\omega}_{N/I}^N = \boldsymbol{\omega}_{E/I}^N + \boldsymbol{\omega}_{N/E}^N = \omega_e \begin{bmatrix} \cos\lambda \\ 0 \\ -\sin\lambda \end{bmatrix} + \begin{bmatrix} \frac{v_E}{R_\Phi + h} \\ -\frac{v_N}{R_\lambda + h} \\ -\frac{v_E \tan\lambda}{R_\Phi + h} \end{bmatrix} \tag{25}$$

The acceleration in the NED frame is related to the acceleration in the body-frame from the relationship

$$\mathbf{a}^N \equiv \begin{bmatrix} a_N \\ a_E \\ a_D \end{bmatrix} = A_B^N(\mathbf{q})\mathbf{a}^B \tag{26}$$

Note that $A_B^N(\mathbf{q})$ is the matrix transpose of $A_N^B(\mathbf{q})$.

V. Wheel Speed Sensor Model

The model used to find the measurements for the speed of each of the rear wheels assumes the velocity in heading direction of the vehicle is entirely in the first component of the fixed in the body frame, so that

$$\mathbf{v}^B = \begin{bmatrix} 2C_1 V_b \\ 0 \\ 0 \end{bmatrix} \tag{27}$$

where C_1 is a constant that defines the time increment in which the number of wheel rotations are to be counted, and V_b is an interim variable which takes the average value of the left/right wheel speeds and radii size. These variables are given by

$$C_1 = \frac{\pi}{100 \text{ (sec)}} \tag{28a}$$

$$V_b = \frac{r_L|L| + r_R|R|}{2} \tag{28b}$$

where r_L and r_R are the respective left and right wheel radii, and $|L|$ and $|R|$ are the respective left and right wheel counts. Note that in the present research all wheel speeds measurements are found as the number of rotations per 100 seconds as defined in Eq. (28a). Due to the wheel speeds being tightly coupled, the wheel count per 100 seconds is the direct sensor measurement used in the filter and the wheel radii must be included as states. The velocity is next converted to the NED frame using the attitude matrix calculated from the quaternion:

$$\mathbf{v}^N \equiv \begin{bmatrix} v_N \\ v_E \\ v_D \end{bmatrix} = A_B^N(\mathbf{q})\mathbf{v}^B \tag{29}$$

The wheel count sensors also give the additional information of the yaw rate based on the difference in wheel rotation counts on the right and left side of the vehicle.

$$\dot{\psi} = 2C_1 \frac{r_L|L| - r_R|R|}{b} \tag{30}$$

In this equation $b = 1$ (m) and is the half length of the vehicle's rear axle. The yaw rate can be related to the attitude of the vehicle by converting the rotation to the angular rate between the NED and body-frame by using the attitude kinematics relationship. This relationship is

$$\begin{bmatrix} \dot{\phi} \\ \dot{\theta} \\ \dot{\psi} \end{bmatrix} = S^{-1}(\phi, \theta)\boldsymbol{\omega}_{B/N}^B \tag{31a}$$

$$S^{-1}(\phi, \theta) = \begin{bmatrix} 1 & \sin\phi\tan\theta & \cos\phi\tan\theta \\ 0 & \cos\phi & -\sin\phi \\ 0 & \sin\phi\sec\theta & \cos\phi\sec\theta \end{bmatrix} \tag{31b}$$

Using this model the measurements for the wheel count on the left and right side can be determined:

$$|L| = \frac{1}{2C_1 r_L}\{A_N^B(1,1)v_N + A_N^B(1,2)v_E + A_N^B(1,3)v_D\} + \frac{b}{4C_1 r_L}(\sin\phi\sec\theta\,\omega_2 + \cos\phi\sec\theta\,\omega_3) \tag{32a}$$

$$|R| = \frac{1}{2C_1 r_R}\{A_N^B(1,1)v_N + A_N^B(1,2)v_E + A_N^B(1,3)v_D\} - \frac{b}{4C_1 r_R}(\sin\phi\sec\theta\,\omega_2 + \cos\phi\sec\theta\,\omega_3) \tag{32b}$$

where $A_N^B(i,j)$ is the i-j^{th} element of A_N^B.

VI. Estimation Vector, Measurement Vector and System Model

The estimation vector for this study has 18 states, representing attitude, position, velocity, inertial sensor bias and wheel radii. When the alternate attitude parameterization of Euler angles are used, the four quaternion states are represented in three angles such as in the results section of this paper. The following vector displays these states:

$$\hat{\mathbf{x}} \equiv \begin{bmatrix} \mathbf{q} \\ \mathbf{p} \\ \mathbf{v}^N \\ \mathbf{b}_g \\ \mathbf{b}_a \\ r_L \\ r_R \end{bmatrix} \tag{33}$$

The attitude matrix from the body to NED frame is represented by the four states of a quaternion parameterization, $\mathbf{q}$. Position has three states and is given in geodetic coordinates, $\mathbf{p} \equiv [\lambda \;\; \Phi \;\; h]^T$. Velocity also consists of three states and is in the NED frame, $\mathbf{v}^N$. Both the rate gyroscope and accelerometer each have three states representing the biases ,$\mathbf{b}_g$ and $\mathbf{b}_a$. The left and right wheel radii are the two remaining states, r_L and r_R. Measurements for 17-state filter are given by

$$\tilde{\mathbf{y}} \equiv \begin{bmatrix} \tilde{\mathbf{p}}_{GPS} \\ \tilde{\boldsymbol{\omega}}_{B/I}^B \\ \tilde{\mathbf{a}}^B \\ |\tilde{L}| \\ |\tilde{R}| \end{bmatrix} \tag{34}$$

The system model is used by the filters for estimating the states from the measurements, predicting the covariance of the filter and to demonstrate observability. For the combined GPS/INS/wheel speed sensor the following equations represent the model used to propagate the states.

$$\dot{\hat{\mathbf{q}}} = \frac{1}{2}\Xi(\hat{\mathbf{q}})\hat{\boldsymbol{\omega}}_{B/N}^B \tag{35a}$$

$$\dot{\hat{\lambda}} = \frac{\hat{v}_N}{\hat{R}_\lambda + \hat{h}} \tag{35b}$$

$$\dot{\hat{\Phi}} = \frac{\hat{v}_E}{(\hat{R}_\Phi + \hat{h})\cos\hat{\lambda}} \tag{35c}$$

$$\dot{\hat{h}} = -\hat{v}_D \tag{35d}$$

$$\dot{\hat{v}}_N = -\Big[\frac{\hat{v}_E}{(\hat{R}_\Phi + \hat{h})\cos\hat{\lambda}} + 2\omega_e\Big]\hat{v}_E\sin\hat{\lambda} + \frac{\hat{v}_N\hat{v}_D}{\hat{R}_\lambda + \hat{h}} + \hat{a}_N \tag{35e}$$

$$\dot{\hat{v}}_E = -\Big[\frac{\hat{v}_E}{(\hat{R}_\Phi + \hat{h})\cos\hat{\lambda}} + 2\omega_e\Big]\hat{v}_N\sin\hat{\lambda} + \frac{\hat{v}_E\hat{v}_D}{\hat{R}_\Phi + \hat{h}} + 2\omega_e\hat{v}_D\cos\hat{\lambda} + \hat{a}_E \tag{35f}$$

$$\dot{\hat{v}}_D = -\frac{\hat{v_E}^2}{\hat{R}_\Phi + \hat{h}} - \frac{\hat{v_N}^2}{\hat{R}_\lambda + \hat{h}} - 2\omega_e\hat{v}_E\cos\hat{\lambda} + \hat{g} + \hat{a}_D \tag{35g}$$

$$\dot{\hat{\mathbf{b}}}_g = \mathbf{0} \tag{35h}$$

$$\dot{\hat{\mathbf{b}}}_a = \mathbf{0} \tag{35i}$$

$$\dot{\hat{r}}_L = 0 \tag{35j}$$

$$\dot{\hat{r}}_R = 0 \tag{35k}$$

A 15-state filter is also used that does not incorporate wheel speed measurements. Wheel radii are not estimated in this filter. The state and measurement vectors for this filter is given by

$$\hat{\mathbf{x}} \equiv \begin{bmatrix} \mathbf{q} \\ \mathbf{p} \\ \mathbf{v}^N \\ \mathbf{b}_g \\ \mathbf{b}_a \end{bmatrix}, \quad \tilde{\mathbf{y}} \equiv \begin{bmatrix} \tilde{\mathbf{p}}_{GPS} \\ \tilde{\boldsymbol{\omega}}^B_{B/I} \\ \tilde{\mathbf{a}}^B \end{bmatrix} \tag{36}$$

This filter is used to compare the results with and without wheel speed measurements.

Table 2. Extended Kalman Filter for GPS/INS/Wheel Speed Sensor Estimation

Initialize	$\hat{\mathbf{x}}(t_0) = \hat{\mathbf{x}}_0$ $P(t_0) = P_0$
Gain	$K_k = P_k^- H_k^T [H_k P_k^- H_k^T + R_k]^{-1}$
Update	$P_k^+ = [I - K_k H_k] P_k^-$ $\Delta\hat{\mathbf{x}}_k^+ = K_k[\tilde{\mathbf{p}}_k - \hat{\mathbf{p}}_k^-]$ $\hat{\mathbf{q}}_k^+ = \hat{\mathbf{q}}_k^- + \frac{1}{2}\Xi(\hat{\mathbf{q}}_k^-)\boldsymbol{\delta\hat{\alpha}}_k^+$ $\hat{\mathbf{p}}_k^+ = \hat{\mathbf{p}}_k^- + \Delta\hat{\mathbf{p}}_k^+$ $\hat{\mathbf{v}}_k^{N+} = \hat{\mathbf{v}}_k^{N-} + \Delta\hat{\mathbf{v}}_k^{N+}$ $\hat{\mathbf{b}}_{gk}^+ = \hat{\mathbf{b}}_{gk}^- + \Delta\hat{\mathbf{b}}_{gk}^+$ $\hat{\mathbf{b}}_{ak}^+ = \hat{\mathbf{b}}_{ak}^- + \Delta\hat{\mathbf{b}}_{ak}^+$ $\hat{r}_L^+ = \hat{r}_L^- + \Delta\hat{r}_L^+$ $\hat{r}_R^+ = \hat{r}_R^- + \Delta\hat{r}_R^+$
Propagation	$\hat{\boldsymbol{\omega}}^B_{B/N} = \tilde{\boldsymbol{\omega}}^B_{B/I} - \hat{\mathbf{b}}_g - A^B_N(\hat{\mathbf{q}})\boldsymbol{\omega}^N_{N/i}$ $\dot{\hat{\mathbf{q}}} = \frac{1}{2}\Xi(\hat{\mathbf{q}})\hat{\omega}^B_{B/N}$ $\hat{\mathbf{a}}^B = \tilde{\mathbf{a}}^B - \hat{\mathbf{b}}_a$ $\dot{\hat{\mathbf{p}}} = \mathbf{f}_p(\hat{\mathbf{p}}, \hat{\mathbf{v}}^N)$ $\dot{\hat{\mathbf{v}}}^N = \mathbf{f}_v(\hat{\mathbf{p}}, \hat{\mathbf{v}}^N) + \hat{\mathbf{a}}^N$ $\dot{P} = FP + PF^T + GQG^T$

VII. Extended Kalman Filter Design

The 17-state EKF estimation algorithm for the GPS/INS/wheel speed sensor combination is summarized in Table 2. This design uses the GPS position measurements loosely coupled and the wheel speed sensor measurements tightly coupled. The state-error, process noise vector and process noise covariance matrix

used in the EKF estimation algorithm are defined as

$$\Delta\mathbf{x} \equiv \begin{bmatrix} \boldsymbol{\delta\alpha} \\ \Delta\mathbf{p} \\ \Delta\mathbf{v}^N \\ \Delta\mathbf{b}_g \\ \Delta\mathbf{b}_a \\ \Delta r_L \\ \Delta r_R \end{bmatrix}, \quad \mathbf{w} \equiv \begin{bmatrix} \boldsymbol{\eta}_{gv} \\ \boldsymbol{\eta}_{gu} \\ \boldsymbol{\eta}_{av} \\ \boldsymbol{\eta}_{au} \end{bmatrix}, \quad Q = \begin{bmatrix} \sigma_{gv}^2 I_{3\times3} & 0_{3\times3} & 0_{3\times3} & 0_{3\times3} \\ 0_{3\times3} & \sigma_{gu}^2 I_{3\times3} & 0_{3\times3} & 0_{3\times3} \\ 0_{3\times3} & 0_{3\times3} & \sigma_{av}^2 I_{3\times3} & 0_{3\times3} \\ 0_{3\times3} & 0_{3\times3} & 0_{3\times3} & \sigma_{au}^2 I_{3\times3} \end{bmatrix} \tag{37}$$

where $\boldsymbol{\delta\alpha}$ is the incremental attitude error.[18]

The sensitivity matrix for the EKF is defined as the partial derivatives of the states related to the measurements, given by

$$H_k = \begin{bmatrix} 0_{3\times3} & \frac{\partial \mathbf{p}_{\text{ECEF}}}{\partial \mathbf{p}_{\text{LLH}}} & 0_{3\times3} & 0_{3\times3} & 0_{3\times3} & 0_{3\times1} & 0_{3\times1} \\ \frac{\partial|L|}{\partial\alpha} & 0_{1\times3} & \frac{\partial|L|}{\partial\mathbf{v}^N} & 0_{1\times3} & 0_{1\times3} & \frac{\partial|L|}{\partial r_L} & \frac{\partial|L|}{\partial r_R} \\ \frac{\partial|R|}{\partial\alpha} & 0_{1\times3} & \frac{\partial|R|}{\partial\mathbf{v}^N} & 0_{1\times3} & 0_{1\times3} & \frac{\partial|R|}{\partial r_L} & \frac{\partial|R|}{\partial r_R} \end{bmatrix} \tag{38}$$

The partial derivatives of the position in ECEF coordinates with respect to the position in geodetic coordinates are found from a covariance mapping between these two coordinate systems, given by Ref. 6:

$$\frac{\partial \mathbf{p}_{\text{ECEF}}}{\partial \mathbf{p}_{\text{LLH}}} = \begin{bmatrix} \frac{\partial N}{\partial\lambda}\cos\lambda\cos\Phi - (N+h)\sin\lambda\cos\Phi & -(N+h)\cos\lambda\sin\Phi & \cos\lambda\cos\Phi \\ \frac{\partial N}{\partial\lambda}\cos\lambda\sin\Phi - (N+h)\sin\lambda\sin\Phi & (N+h)\cos\lambda\cos\Phi & \cos\lambda\sin\Phi \\ \frac{\partial N}{\partial\lambda}(1-e^2)\sin\lambda + [N(1-e^2)+h]\cos\lambda & 0 & \sin\lambda \end{bmatrix} \tag{39}$$

where

$$\frac{\partial N}{\partial\lambda} = \frac{ae^2\sin\lambda\cos\lambda}{(1-e^2\sin^2\lambda)^{3/2}} \tag{40}$$

The partial derivatives with respect to each of the states in this matrix are found for the left wheel from the wheel count measurement equation. A perturbation approach is used to approximate the partial derivatives for components of the attitude matrix.[18] This approach uses Eq. (41) to find the partial derivatives directly from attitude matrix components as opposed to taking partial derivatives of the Euler angle components from Eq. (3):

$$\frac{\Delta\mathbf{v}^B}{\boldsymbol{\delta\alpha}} = [A_N^B(\hat{\mathbf{q}})\mathbf{v}^N\times] \tag{41}$$

Using this approach the partial derivatives are

$$\frac{\partial|L|}{\partial\phi} = \frac{b}{4C_1r_L}(\cos\phi\sec\theta\,\omega_2 - \sin\phi\sec\theta\,\omega_3) \tag{42a}$$

$$\frac{\partial|L|}{\partial\theta} = \frac{b}{4C_1r_L}(\sin\phi\sec\theta\tan\theta\,\omega_2 + \cos\phi\sec\theta\tan\theta\,\omega_3) - \frac{1}{2C_1r_L}(A_N^B(3,1)v_N + A_N^B(3,2)v_E + A_N^B(3,3)v_D) \tag{42b}$$

$$\frac{\partial|L|}{\partial\psi} = \frac{1}{2C_1r_L}(A_N^B(2,1)v_N + A_N^B(2,2)v_E + A_N^B(2,3)v_D) \tag{42c}$$

$$\frac{\partial|L|}{\partial\boldsymbol{\alpha}} = \begin{bmatrix} \frac{\partial|L|}{\partial\phi} & \frac{\partial|L|}{\partial\theta} & \frac{\partial|L|}{\partial\psi} \end{bmatrix} \tag{42d}$$

$$\frac{\partial|L|}{\partial v_N} = \frac{A_B^N(1,1)}{2C_1r_L}, \qquad \frac{\partial|L|}{\partial v_E} = \frac{A_B^N(1,2)}{2C_1r_L}, \qquad \frac{\partial|L|}{\partial v_D} = \frac{A_B^N(1,3)}{2C_1r_L} \tag{42e}$$

$$\frac{\partial|L|}{\partial\mathbf{v}^N} = \begin{bmatrix} \frac{\partial|L|}{\partial v_N} & \frac{\partial|L|}{\partial v_E} & \frac{\partial|L|}{\partial v_D} \end{bmatrix} \tag{42f}$$

$$\frac{\partial|L|}{\partial r_L} = \frac{-1}{2C_1r_L^2}(A_N^N(1,1)v_N + A_B^N(1,2)v_E + A_B^N(1,3)v_D) + \frac{-b}{2C_1r_L^2}(\sin\phi\sec\theta\omega_2 + \cos\phi\sec\theta\omega_3) \tag{42g}$$

$$\frac{\partial |L|}{\partial r_R} = 0 \tag{42h}$$

Similarly the partial derivatives for the right wheel are

$$\frac{\partial |R|}{\partial \phi} = \frac{-b}{4C_1 r_R}(\cos\phi \sec\theta \omega_2 - \sin\phi \sec\theta \omega_3) \tag{43a}$$

$$\frac{\partial |R|}{\partial \theta} = \frac{-b}{4C_1 r_R}(\sin\phi \sec\theta \tan\theta \omega_2 + \cos\phi \sec\theta \tan\theta \omega_3) - \frac{1}{2C_1 r_R}(A_N^B(3,1)v_N + A_N^B(3,2)v_E + A_N^B(3,3)v_D) \tag{43b}$$

$$\frac{\partial |R|}{\partial \psi} = \frac{1}{2C_1 r_R}(A_N^B(2,1)v_N + A_N^B(2,2)v_E + A_N^B(2,3)v_D) \tag{43c}$$

$$\frac{\partial |R|}{\partial \alpha} = \begin{bmatrix} \frac{\partial |R|}{\partial \phi} & \frac{\partial |R|}{\partial \theta} & \frac{\partial |R|}{\partial \psi} \end{bmatrix} \tag{43d}$$

$$\frac{\partial |R|}{\partial v_N} = \frac{A_B^N(1,1)}{2C_1 r_R}, \qquad \frac{\partial |R|}{\partial v_E} = \frac{A_B^N(1,2)}{2C_1 r_R}, \qquad \frac{\partial |R|}{\partial v_D} = \frac{A_B^N(1,3)}{2C_1 r_R} \tag{43e}$$

$$\frac{\partial |R|}{\partial \mathbf{v}^N} = \begin{bmatrix} \frac{\partial |R|}{\partial v_N} & \frac{\partial |R|}{\partial v_E} & \frac{\partial |R|}{\partial v_D} \end{bmatrix} \tag{43f}$$

$$\frac{\partial |R|}{\partial r_R} = \frac{-1}{2C_1 r_R^2}(A_N^N(1,1)v_N + A_B^N(1,2)v_E + A_B^N(1,3)v_D) + \frac{b}{2C_1 r_R^2}(\sin\phi \sec\theta \omega_2 + \cos\phi \sec\theta \omega_3) \tag{43g}$$

$$\frac{\partial |R|}{\partial r_L} = 0 \tag{43h}$$

The error dynamics for the EKF propagation are given as

$$\Delta \dot{\mathbf{x}} = F \Delta \mathbf{x} + G \mathbf{w} \tag{44}$$

of which the F and G matrices are defined as

$$F = \begin{bmatrix} F_{11} & F_{12} & F_{13} & -I_{3\times3} & 0_{3\times3} & 0_{1\times3} & 0_{1\times3} \\ 0_{3\times3} & F_{22} & F_{23} & 0_{3\times3} & 0_{3\times3} & 0_{1\times3} & 0_{1\times3} \\ F_{31} & F_{32} & F_{33} & 0_{3\times3} & F_{35} & 0_{1\times3} & 0_{1\times3} \\ 0_{3\times3} & 0_{3\times3} & 0_{3\times3} & 0_{3\times3} & 0_{3\times3} & 0_{1\times3} & 0_{1\times3} \\ 0_{3\times3} & 0_{3\times3} & 0_{3\times3} & 0_{3\times3} & 0_{3\times3} & 0_{1\times3} & 0_{1\times3} \\ 0_{3\times1} & 0_{3\times1} & 0_{3\times1} & 0_{3\times1} & 0_{3\times1} & 0 & 0 \\ 0_{3\times1} & 0_{3\times1} & 0_{3\times1} & 0_{3\times1} & 0_{3\times1} & 0 & 0 \end{bmatrix} \tag{45}$$

$$G = \begin{bmatrix} -I_{3\times3} & 0_{3\times3} & 0_{3\times3} & 0_{3\times3} \\ 0_{3\times3} & 0_{3\times3} & 0_{3\times3} & 0_{3\times3} \\ 0_{3\times3} & 0_{3\times3} & -A_B^N(\hat{\mathbf{q}}) & 0_{3\times3} \\ 0_{3\times3} & I_{3\times3} & 0_{3\times3} & 0_{3\times3} \\ 0_{3\times3} & 0_{3\times3} & 0_{3\times3} & I_{3\times3} \\ 0_{1\times3} & 0_{1\times3} & 0_{1\times3} & 0_{1\times3} \\ 0_{1\times3} & 0_{1\times3} & 0_{1\times3} & 0_{1\times3} \end{bmatrix} \tag{46}$$

The components of the F matrix are

$$F_{11} = -[(\tilde{\boldsymbol{\omega}}_{B/I}^B - \hat{\mathbf{b}}_g)\times], \qquad F_{12} = -A_N^B(\hat{\mathbf{q}}) \frac{\partial \boldsymbol{\omega}_{N/I}^N}{\partial \mathbf{p}}\Big|_{\hat{\mathbf{p}},\hat{\mathbf{v}}^N}, \qquad F_{13} = -A_N^B(\hat{\mathbf{q}}) \frac{\partial \boldsymbol{\omega}_{N/I}^N}{\partial \mathbf{v}^N}\Big|_{\hat{\mathbf{p}}} \tag{47a}$$

$$F_{22} = \frac{\partial \dot{\mathbf{p}}}{\partial \mathbf{p}}\Big|_{\hat{\mathbf{p}},\hat{\mathbf{v}}^N}, \qquad F_{23} = \frac{\partial \dot{\mathbf{p}}}{\partial \mathbf{v}^N}\Big|_{\hat{\mathbf{p}}} \tag{47b}$$

$$F_{31} = -A_N^B(\hat{\mathbf{q}})[\hat{\mathbf{a}}^B\times], \qquad F_{32} = \frac{\partial \dot{\mathbf{v}}^N}{\partial \mathbf{p}}\Big|_{\hat{\mathbf{p}},\hat{\mathbf{v}}^N}, \qquad F_{33} = \frac{\partial \dot{\mathbf{v}}^N}{\partial \mathbf{v}^N}\Big|_{\hat{\mathbf{p}},\hat{\mathbf{v}}^N}, \qquad F_{35} = -A_N^B(\hat{\mathbf{q}}) \tag{47c}$$

In these components the partial derivatives for position are

$$\frac{\partial \dot{\mathbf{p}}}{\partial \mathbf{p}} = \begin{bmatrix} \frac{v_N}{(R_\lambda+h)^2}\frac{\partial R_\lambda}{\partial \lambda} & 0 & -\frac{v_N}{(R_\lambda+h)^2} \\ -\frac{v_E \sec\lambda}{(R_\Phi+h)^2}\frac{\partial R_\Phi}{\partial \lambda} + \frac{v_E \sec\lambda \tan\lambda}{R_\Phi+h} & 0 & -\frac{v_E \sec\lambda}{(R_\Phi+h)^2} \\ 0 & 0 & 0 \end{bmatrix} \tag{48}$$

$$\frac{\partial \dot{\mathbf{p}}}{\partial \mathbf{v}^N} = \begin{bmatrix} \frac{1}{R_\lambda+h} & 0 & 0 \\ 0 & \frac{\sec\lambda}{R_\Phi+h} & 0 \\ 0 & 0 & -1 \end{bmatrix} \tag{49}$$

and the partial derivatives for velocity are given by

$$\frac{\partial \dot{\mathbf{v}}^N}{\partial \mathbf{p}} = \begin{bmatrix} Y_{11} & 0 & Y_{13} \\ Y_{21} & 0 & Y_{23} \\ Y_{31} & 0 & Y_{33} \end{bmatrix}, \qquad \frac{\partial \dot{\mathbf{v}}^N}{\partial \mathbf{v}^N} = \begin{bmatrix} Z_{11} & Z_{12} & Z_{13} \\ Z_{21} & Z_{22} & Z_{23} \\ Z_{31} & Z_{32} & 0 \end{bmatrix} \tag{50}$$

where

$$Y_{11} = -\frac{v_E^2 \sec^2\lambda}{R_\Phi+h} + \frac{v_E^2 \tan\lambda}{(R_\Phi+h)^2}\frac{\partial R_\Phi}{\partial \lambda} - 2\omega_e v_E \cos\lambda - \frac{v_N v_D}{(R_\lambda+h)^2}\frac{\partial R_\lambda}{\partial \lambda} \tag{51a}$$

$$Y_{13} = \frac{v_E^2 \tan\lambda}{(R_\Phi+h)^2} - \frac{v_E v_D}{(R_\lambda+h)^2} \tag{51b}$$

$$Y_{21} = \frac{v_E v_N \sec^2\lambda}{R_\Phi+h} - \frac{v_E v_N \tan\lambda}{(R_\Phi+h)^2}\frac{\partial R_\Phi}{\partial \lambda} + 2\omega_e v_N \cos\lambda - \frac{v_E v_D}{(R_\Phi+h)^2}\frac{\partial R_\Phi}{\partial \lambda} - 2\omega_e v_D \sin\lambda \tag{51c}$$

$$Y_{23} = -v_E\big[\frac{v_N \tan\lambda + v_D}{(R_\Phi+h)^2)}\big] \tag{51d}$$

$$Y_{31} = \frac{v_E^2}{(R_\Phi+h)^2}\frac{\partial R_\Phi}{\partial \lambda} + \frac{v_N^2}{(R_\lambda+h)^2}\frac{\partial R_\lambda}{\partial \lambda} + 2\omega_e v_E \sin\lambda + \frac{\partial g}{\partial \lambda} \tag{51e}$$

$$Y_{33} = \frac{v_E^2}{(R_\Phi+h)^2} + \frac{v_N^2}{(R_\lambda+h)^2} + \frac{\partial g}{\partial \lambda} \tag{51f}$$

and

$$Z_{11} = \frac{v_D}{R_\lambda+h}, \qquad Z_{12} = -\frac{2v_E \tan\lambda}{R_\Phi+h} + 2\omega_e \sin\lambda \qquad Z_{12} = \frac{v_N}{R_\lambda+h} \tag{52a}$$

$$Z_{21} = \frac{2v_E \tan\lambda}{R_\Phi+h} + 2\omega_e \sin\lambda, \qquad Z_{22} = \frac{v_D + v_N \tan\lambda}{R_\Phi+h}, \qquad Z_{23} = \frac{v_E}{R_\Phi+h} + 2\omega_e \cos\lambda \tag{52b}$$

$$Z_{31} = -\frac{2v_N}{R_\lambda+h}, \qquad Z_{32} = -\frac{2v_E}{R_\Phi+h} - 2\omega_e \cos\lambda \tag{52c}$$

with the partial derivatives for local gravity given by

$$\frac{\partial g}{\partial \lambda} = 9.780327[1.06048\times10^{-2}\sin\lambda\cos\lambda - 4.64\times10^{-5}(\sin\lambda\cos^3\lambda - \sin^3\lambda\cos\lambda)] + 8.8\times10^{-9}h\sin\lambda\cos\lambda \tag{53a}$$

$$\frac{\partial g}{\partial h} = -3.0877\times10^{-6} + 4.4\times10^{-9}\sin^2\lambda + 1.44\times10^{-13}h \tag{53b}$$

In the estimation algorithm the assumed measurements for position from the GPS are modeled by

$$\tilde{\mathbf{p}}_k = \mathbf{p}_k + \mathbf{v}_k \tag{54}$$

where $\mathbf{v}_k$ is a zero-mean Gaussian noise process with covariance R_k. The filter is first initialized with a known state (the bias initial conditions for the gyro and accelerometer are usually assumed zero) and the error-covariance matrix. The first three diagonal elements of the error-covariance matrix correspond to the attitude errors. Then, the Kalman gain is computed using the measurement-error covariance R_k and the sensitivity matrix. The state error-covariance follows the standard EKF update. The position, velocity,

bias and wheel radius states also follow the standard EKF additive correction while the attitude error-state update is computed using a multiplicative update.[18] The updated quaternion is re-normalized by brute force. The propagation equations follow the standard EKF model.

The $\dot{P}$ equation for the propagation of the covariance can be approximated by using discrete time propagation given by

$$P_{k+1}^{-} = \Phi_k P_k^{+} \Phi_k^T + \mathcal{Q}_k \tag{55}$$

In this equation $\mathcal{Q}_k$ is the discrete time covariance matrix and Φ_k is the transition matrix. These can be numerically solved for by using Moler and Van Loon.[19] In this procedure the following $(2n \times 2n)$ matrix if first found:

$$\mathcal{A} = \begin{bmatrix} -F & GQG^T \\ 0 & F^T \end{bmatrix} \Delta t \tag{56}$$

From $\mathcal{A}$ the matrix exponential is computed:

$$\mathcal{B} = e^{\mathcal{A}} \equiv \begin{bmatrix} \mathcal{B}_{11} & \mathcal{B}_{12} \\ 0 & \mathcal{B}_{22} \end{bmatrix} = \begin{bmatrix} \mathcal{B}_{11} & \Phi_k^{-1}\mathcal{Q}_k \\ 0 & \Phi_k^T \end{bmatrix} \tag{57}$$

From this equation the state transition matrix can be found from

$$\Phi_k = \mathcal{B}_{22}^T \tag{58}$$

and process noise covariance found from

$$\mathcal{Q}_k = \Phi_k \mathcal{B}_{12} \tag{59}$$

VIII. Unscented Filter Design

The filter presented is from Wan,[20] derived for discrete-time nonlinear equations, in which the system model is given as

$$\mathbf{x}_{k+1} = \mathbf{f}(\mathbf{x}_k, k) + \mathbf{w}_k \tag{60a}$$

$$\tilde{\mathbf{y}} = \mathbf{h}(\mathbf{x}_k, k) + \mathbf{v}_k \tag{60b}$$

A continuous-time model can be written using Eq. (60a) with an appropriate numerical integration scheme. It is assumed that $\mathbf{w}_k$ and $\mathbf{v}_k$ are zero-mean Gaussian noise processes with covariance given by $\mathcal{Q}_k$ and R_k respectively. First the Kalman filter update equation is rewritten as[21]

$$\hat{\mathbf{x}}_k^{+} = \hat{\mathbf{x}}_k^{-} + K_k \boldsymbol{\upsilon}_k \tag{61a}$$

$$P_k^{+} = P_k^{-} + K_k P_k^{\upsilon\upsilon} K_k^T \tag{61b}$$

where $\boldsymbol{\upsilon}_k$ is the innovations process given by

$$\boldsymbol{\upsilon}_k \equiv \tilde{\mathbf{y}}_k - \hat{\mathbf{y}}_k^{-} \tag{62a}$$

$$= \tilde{\mathbf{y}}_k - \mathbf{h}(\hat{\mathbf{x}}_k^{-}, k) \tag{62b}$$

The covariance of $\boldsymbol{\upsilon}_k$ is defined as $P_k^{\nu\nu}$. The gain K_k is next found:

$$K_k = P_k^{xy} (P_k^{\upsilon\upsilon})^{-1} \tag{63}$$

where P_k^{xy} is the cross-correlation covariance between $\hat{\mathbf{x}}_k^{-}$ and $\hat{\mathbf{y}}_k^{-}$.

The propagation equations begin with the calculation of the sigma points:

$$\boldsymbol{\sigma}_k \leftarrow 2n \text{ columns from} \pm \sqrt{P_k^{+} + \bar{Q}_k} \tag{64a}$$

$$\boldsymbol{\chi}_k(0) = \hat{\mathbf{x}}_k^{+} \tag{64b}$$

$$\boldsymbol{\chi}_{k+1}(i) = \boldsymbol{\sigma}_k(i) + \hat{\mathbf{x}}_k^{+} \tag{64c}$$

Note that there are now a total of $2n$ sets of sigma points $\boldsymbol{\sigma}_k$, from the positive and negative square roots. Each set of sigma points is evaluated through

$$\boldsymbol{\chi}_{k+1}(i) = \mathbf{f}[\boldsymbol{\chi}_k(i), k] \tag{65}$$

The sigma points are combined to find the predicted mean for the state estimate by using a weighted sum of $\boldsymbol{\chi}_{k+1}(i)$, given by

$$\hat{\mathbf{x}}_{k+1}^{-} = \sum_{i=0}^{2n} W_i^{\text{mean}} \boldsymbol{\chi}_{k+1}(i) \tag{66}$$

This predicted mean is now used to find the predicted covariance:

$$P_{k+1}^{-} = \sum_{i=0}^{2n} W_i^{\text{cov}} [\boldsymbol{\chi}_{k+1}(i) - \hat{\mathbf{x}}_{k+1}^{-}][\boldsymbol{\chi}_{k+1}(i) - \hat{\mathbf{x}}_{k+1}^{-}]^T + \bar{Q}_k \tag{67}$$

The mean observation is given as

$$\hat{\mathbf{y}}_{k+1}^{-} = \sum_{i=0}^{2n} W_i^{\text{mean}} \boldsymbol{\gamma}_{k+1}(i) \tag{68}$$

where

$$\boldsymbol{\gamma}_{k+1}(i) = \mathbf{h}[\boldsymbol{\chi}_{k+1}(i), k+1] \tag{69}$$

The output covariance is given as

$$P_{k+1}^{yy} = \sum_{i=0}^{2n} W_i^{\text{cov}} [\boldsymbol{\gamma}_{k+1}(i) - \hat{\mathbf{y}}_{k+1}^{-}][\boldsymbol{\gamma}_{k+1}(i) - \hat{\mathbf{y}}_{k+1}^{-}]^T \tag{70}$$

The innovations covariance can simply be found by

$$P_{k+1}^{\upsilon\upsilon} = P_{k+1}^{yy} + R_{k+1} \tag{71}$$

Lastly the cross-correlation matrix is found from

$$P_{k+1}^{xy} = \sum_{i=0}^{2n} W_i^{\text{cov}} [\boldsymbol{\chi}_{k+1}(i) - \hat{\mathbf{x}}_{k+1}^{-}][\boldsymbol{\gamma}_{k+1}(i) - \hat{\mathbf{y}}_{k+1}^{-}]^T \tag{72}$$

The parameters required in this algorithm are next discussed. The parameter γ is given by the following equation in which λ is a composite scaling parameter:

$$\gamma = \sqrt{n + \lambda} \tag{73a}$$

$$\lambda = \alpha^2 (n + \kappa) - n \tag{73b}$$

In this equation α is a constant which determines the spread of the sigma points and is set to a small positive number between, $1 \times 10^{-4} \leq \alpha \leq 1$. The scalar κ is chosen to be $\kappa = n - 3$ which minimizes mean-squared-error to fourth order.

The weights used in the covariance calculations are found from

$$W_0^{\text{mean}} = \frac{\lambda}{n + \lambda} \tag{74a}$$

$$W_0^{\text{cov}} = \frac{\lambda}{n + \lambda} + (1 - \alpha^2 + \beta) \tag{74b}$$

$$W_i^{mean} = W_i^{\text{cov}} = \frac{1}{2(n + \lambda)}, \quad i = 1, 2, ..., 34 \tag{74c}$$

Similarly to the EKF the Unscented filter requires the calculation of the discrete time state transition matrix and covariance noise matrix to add the process noise in the filter. This requires that the F and G matrix be calculated. The equation used to calculate the process noise is as follows:

$$\Phi(\Delta t) \bar{Q}_k \Phi^T(\Delta t) + \bar{Q}_k = \mathcal{Q}_k \tag{75}$$

This equation is known as the discrete time Sylvester equation and is solved with a Bartels-Stewert numerical algorithm.[22]

A. Unscented Filter Design for GPS/INS/Wheel Speed Sensors

This section discusses deriving the UF for specific GPS/INS/wheel speed sensor application. The estimation algorithm follows closely the UF filter description above, with a quaternion normalization procedure. When the predicted quaternion mean is derived using the averaged sum of quaternions the resulting quaternion may not have unit norm. This creates a situation in which the straightforward calculation in the UF is undesirable for the quaternion. A three-component vector representing an attitude error is used instead.

To begin the state vector is defined as

$$\boldsymbol{\chi}_k(0) = \hat{\mathbf{x}}_k^+ \equiv \begin{bmatrix} \boldsymbol{\delta}\hat{\mathbf{s}}_k^+ \\ \hat{\mathbf{p}}_k^+ \\ \hat{\mathbf{p}}_k^{N+} \\ \hat{\mathbf{b}}_g \\ \hat{\mathbf{b}}_a \\ \hat{r_L} \\ \hat{r_R} \end{bmatrix}, \quad \boldsymbol{\chi}_k(i) \equiv \begin{bmatrix} \boldsymbol{\chi}_k^{\delta s}(i) \\ \boldsymbol{\chi}_k^{p}(i) \\ \boldsymbol{\chi}_k^{v^N}(i) \\ \boldsymbol{\chi}_k^{b_g}(i) \\ \boldsymbol{\chi}_k^{b_a}(i) \\ \chi_k^{r_L}(i) \\ \chi_k^{r_R}(i) \end{bmatrix} \tag{76}$$

where $\boldsymbol{\delta}\hat{\mathbf{s}}_k^+$ is a generalized Rodrigues error-vector,[23] used in propagating and update of the nominal quaternion. Because the three-dimensional attitude is unconstrained, the resulting overall covariance matrix is a 17×17 matrix. The three components of the vector $\boldsymbol{\chi}_k(i)$ are defined in Eq. (64) as $\boldsymbol{\chi}_k^{\delta s}(i)$. To describe $\boldsymbol{\chi}_k^{\delta s}$ a new quaternion is generated by multiplying an error quaternion by the current estimate:

$$\hat{\mathbf{q}}_k^+(0) = \hat{\mathbf{q}}_k^+ \tag{77a}$$

$$\hat{\mathbf{q}}_k^+(i) = \boldsymbol{\delta}\hat{\mathbf{q}}_k^+(i) \oplus \hat{\mathbf{q}}_k^+ \tag{77b}$$

where $\boldsymbol{\delta}\mathbf{q}_k^+(i) \equiv \begin{bmatrix} \boldsymbol{\delta}\boldsymbol{\varrho}_k^{+T}(i) & \delta q_{4_k}^{+T}(i) \end{bmatrix}$ represented by[23]

$$\delta q_{4_k}^{+T}(i) = \frac{-a\|\boldsymbol{\chi}_k^{\delta s}(i)\|^2 + f\sqrt{f^2 + (1-a^2)\|\boldsymbol{\chi}_k^{\delta s}(i)\|^2}}{f^2 + \|\boldsymbol{\chi}_k^{\delta s}(i)\|^2}, \quad i = 1, 2..., 34 \tag{78a}$$

$$\boldsymbol{\delta}\boldsymbol{\varrho}_k^+(i) = f^{-1}[a + \delta q_{4_k}^{+T}(i)]\boldsymbol{\chi}_k^{\delta s}(i), \quad i = 1, 2, ..., 34 \tag{78b}$$

The parameter $a = 1$ and the scale factor $f = 2(a+1)$. This sets $\boldsymbol{\chi}_k^{\delta s}$ to give the standard vector of modified Rodrigues error parameters. Equation (77a) requires that the $\boldsymbol{\chi}_k^{\delta s}(0)$ be set to zero. This is due to the reset of the attitude error after the update, which is used to move information from one part of the attitude to another.[24] Next the updated quaternions are propagated forward using Eq. (35a), with

$$\dot{\hat{\mathbf{q}}}(i) = \frac{1}{2}\Xi(\hat{\mathbf{q}})\hat{\boldsymbol{\omega}}_{B/N}^B(i) \tag{79}$$

with the estimates of the angular rates given by

$$\hat{\boldsymbol{\omega}}_{B/N}^B(i) = [\tilde{\boldsymbol{\omega}}_{B/I}^B - \boldsymbol{\chi}^{b_g}(i)] - A_N^B[\hat{\mathbf{q}}(i)]\boldsymbol{\omega}_{N/I}^N, \quad i = 0, 1, ..., 34 \tag{80}$$

where $\boldsymbol{\chi}^{b_g}$ is formed from the gyro bias sigma points. The propagated error quaternions are computed using

$$\boldsymbol{\delta}\mathbf{q}_{k+1}^-(i) = \hat{\mathbf{q}}_{k+1}^-(i) \otimes [\hat{\mathbf{q}}_{k+1}^-(0)]^{-1}, \quad i = 0, 2, ..., 34 \tag{81}$$

Note that $\boldsymbol{\delta}\mathbf{q}_{k+1}^-(0)$ is the identity quaternion. The propagated quaternion is computed using[23]

$$\boldsymbol{\chi}_{k+1}^{\delta s}(0) = \mathbf{0} \tag{82}$$

$$\boldsymbol{\chi}_{k+1}^{\delta s}(i) = f\frac{\boldsymbol{\delta}\boldsymbol{\varrho}_{k+1}^-(i)}{a + \delta q_{4_{k+1}}^-}, \quad i = 1, 2, ..., 34 \tag{83}$$

with $\boldsymbol{\delta}\mathbf{q}_{k+1}^-(i) = \begin{bmatrix} \boldsymbol{\delta}\boldsymbol{\varrho}_{k+1}^{-T}(i) & \delta q_{4_{k+1}}^-(i) \end{bmatrix}^T$. With this the predicted covariance can be computed:

$$\hat{\mathbf{q}}_{k+1}^+ = \boldsymbol{\delta}\mathbf{q}_{k+1}^+ \otimes \mathbf{q}_{k+1}^-(0) \tag{84}$$

$$\delta q_{4_{k+1}}^{+} = \frac{-a\|\boldsymbol{\delta}\hat{\mathbf{s}}_{k+1}^{+}\|^2 + f\sqrt{f^2 + (1-a^2)\|\boldsymbol{\delta}\hat{\mathbf{s}}_{k+1}^{+}\|^2}}{f^2 + \|\boldsymbol{\delta}\hat{\mathbf{s}}_{k+1}^{+}\|^2} \tag{85}$$

$$\boldsymbol{\delta\varrho}_{k+1}^{+} = f^{-1}[a + \delta q_{4_{k+1}}^{+}]\boldsymbol{\delta}\hat{\mathbf{s}}_{k+1}^{+} \tag{86}$$

IX. Simulation Results

In this section results are shown for a simulation run that estimates a moving land vehicle's attitude, position, velocity, rear wheel radii, and biases for the gyro/accelerometer inertial sensors. The total time of each simulation is 5 minutes with a measurement update rate of 0.5 seconds. The gyro and accelerometer noise parameters are $\sigma_{gv} = 2.9089 \times 10^{-7}$ rad/sec$^{1/2}$, $\sigma_{gu} = 9.1989 \times 10^{-7}$ rad/sec$^{3/2}$, $\sigma_{gav} = 9.8100 \times 10^{-5}$ m/sec$^{3/2}$ and $\sigma_{au} = 6.0000 \times 10^{-5}$ m/sec$^{5/2}$ respectfully. The vehicle position is described in geodetic coordinates, with an initial position located in Buffalo, NY at $\lambda_0 = 42.7167$ degrees, $\Phi_0 = 78.8667$ degrees and height above sea level, $h_0 = 150$ meters. The velocity of the vehicle is given in the NED frame, with initially the vehicle being at rest. The initial quaternion of the vehicle is found using the attitude matrix from the NED to body-frame. The GPS constellation[6] uses GPS week 137 at a time of applicability of 61440.000 seconds. The number of available satellites is computed using a 15 degree elevation cutoff angle. The filter requires a minimum of 4 satellites with the loose coupling method used in the filter design. A greater number of satellite signals received results in greater precision of the position measurement. Clock-bias drift is modeled using a random walk process and GPS measurements are found using white-noise errors with a standard deviation of 5 meters.

The land vehicle follows a track shown in Fig 1. The vehicle begins at rest oriented 60 degrees East of North on a flat surface. For 20 seconds the vehicle accelerates in the heading direction at 1.0 m/sec^2. After accelerating the vehicle reaches a velocity of approximately 45 MPH and remains constant for the duration of the simulation. After 0.75 miles the vehicle makes a 90 degree turn, with a roll angle of 1.5 degrees. The vehicle now travels 1.5 miles and again turns 90 degrees. Next the vehicle continues 1 mile and then pitches up to 3 degrees for 20 seconds before leveling back off to flat. The vehicle travels along in this manner, pitching down on the opposite side with the same pattern until reaching the origin position. From this vehicle path information the true states at each time step are found and measured quantities are simulated.

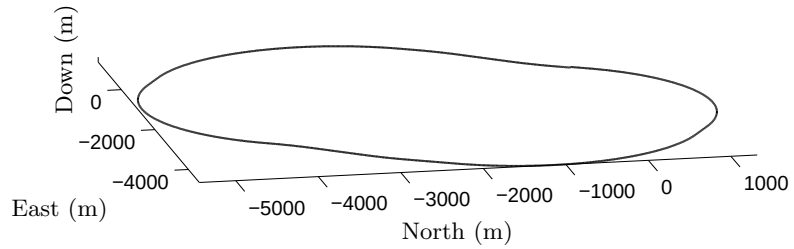

Figure 1. Path Traveled in Vehicle Simulation

The initial conditions for the filter are chosen to simulate road vehicle initial errors. The initial errors chosen mainly stress the EKF, testing the robustness of the filter design. In the EKF the initial covariance matrix is diagonal, with each component representing the square of the expected value of the error in each state. For each filter the initial variance of the attitude is set to a 3σ bound of 15 degrees and initial error values of 7 degrees for the attitude angles. The initial position was set to the true longitude, latitude and

height. The variance for the geodetic angles was set to $(1 \times 10^{-6})^2$ rad^2 and the variance for the height is $(20/3)^2$ m^2. The initial variance for the velocity for North and East are set to $(200/3)^2$ m^2/sec^2 and in the down direction, $(10/3)^2$ m^2/sec^2. The initial gyro and accelerometer biases are set to zero. The variance of the gyro biases are set to a 3σ bound of 30 degrees per hour and the accelerometer biases bounded by 0.005 m/sec^2. The UF uses parameters of $\alpha = 1$, $\beta = 2$ and $\kappa = -3$.

The results of this study compare the use of GPS/INS alone, i.e. the 15-state filter, to the case of GPS/INS with the wheel speed sensors, i.e. the 17-state filter, using both an EKF and UF estimation algorithm. This produces four sets of estimates which are compared for error convergence and robustness. Each estimation run is conducted using the same covariance, initial conditions and set of measurements. The results for the EKF attitude, position and gyro biases are shown in Fig. 2. The attitude results from Fig. 2(a) and Fig. 2(b) show the 3σ bounds for the yaw component converges to a steady value within 10 seconds when the wheel speed sensors are used, over 20 times faster than when GPS/INS is used alone. For the case of only GPS/INS the yaw state is the least observable and with the addition of the wheel speed sensors this limitation is compensated. Additionally from the EKF attitude results the pitch component converges slightly faster and the roll is unaffected by the addition of the wheel speed sensors. The UF results for the states of attitude, position and gyro biases are shown in Fig. 3. The UF attitude filter results from Fig. 3(a) and Fig. 3(b) show the same pattern as the EKF results but with slower convergence overall. In the position results for the EKF comparing Fig. 3(a) and Fig. 3(b), shown is slightly faster initial convergence in all states with the addition of the wheel speed sensors but convergence to a steady 3σ error bound value in the same amount of time for both cases. For the case of position the UF produces very similar results to the EKF as shown in Fig. 3(c) and Fig. 3(d).

From the results it seems the EKF provides overall faster convergence as well as having the benefit of requiring less computational power than the UF. This is true for very small initial state errors, but when testing for filter robustness the UF can handle far larger errors before the error diverges outside the 3σ bounds. When the filters are stressed from increasing initial state errors for the attitude components, especially in yaw, the 15-state EKF could handle much higher initial errors than the 17-state EKF before the estimates diverged. Errors as small as 3 degrees in yaw caused the corresponding error to drift beyond the 3σ bounds. This is seen in Fig. 2(b) for the 17-state EKF yaw component results for when the yaw initial error was set to 7 degrees. For the same initial error values in the 17-state UF from Fig. 3(b) the errors remain within the 3σ bounds. The UF is more robust in handling these initial attitude errors, with similar robustness results in both the 15- and 17-state UF. This indicates that the 17-state UF provides the advantage of faster convergence from the addition of the wheel speed sensors and does not have the decreased robustness as in the 17-state EKF.

X. Conclusion

This paper formulated an estimation algorithm by fusing sensor data from GPS, INS and wheel speed sensors for use in land vehicle navigation applications. Filter results for an EKF and UF were compared for cases of GPS/INS alone and with the addition of wheel speed sensors. Results show faster convergence with the addition of the wheel speed sensors for yaw, pitch and position in both types of filters. The robustness of the EKF with the use of the wheel speed sensors was found to be limited for large initial state errors. The UF filter provides increased performance for cases with large initial state errors along with the faster convergence from the addition of wheel speed sensors to the GPS/INS at the cost of increased computational time.

References

[1]Jekeli, C., *Inertial Navigation Systems with Geodetic Applications*, Walter de Gruyter, Berlin, Germany, 2000.

[2]Parkinson, B. W. and Spilker, J. J., *The Global Positioning System: Theory and Applications*, AIAA, 1996.

[3]Bevly, D. M., "Global Positioning System (GPS): A Low-Cost Velocity Sensor for Correcting Inertial Sensor Errors on Ground Vehicles," *Journal of Dynamic Systems, Measurement, and Control*, Vol. 126, No. 2, June 2004, pp. 255–264.

[4]Abbott, E., Powell, D., Signal, A., and Redmond, W. A., "Land-Vehicle Navigation Using GPS," *Proceedings of the IEEE*, Vol. 87, No. 1, 1999, pp. 145–162.

[5]Bevly, D., Ryu, J., and Gerdes, J. C., "Integrating INS Sensors with GPS Measurements for Continuous Estimation of Vehicle Sideslip, Roll, and Tire Cornering Stiffness," *IEEE Transactions on Intelligent Transportation Systems*, Vol. 7, No. 4, 2006, pp. 483–493.

[6]Crassidis, J. L., "Sigma-Point Kalman Filtering for Integrated GPS and Inertial Navigation," *IEEE Transactions on*

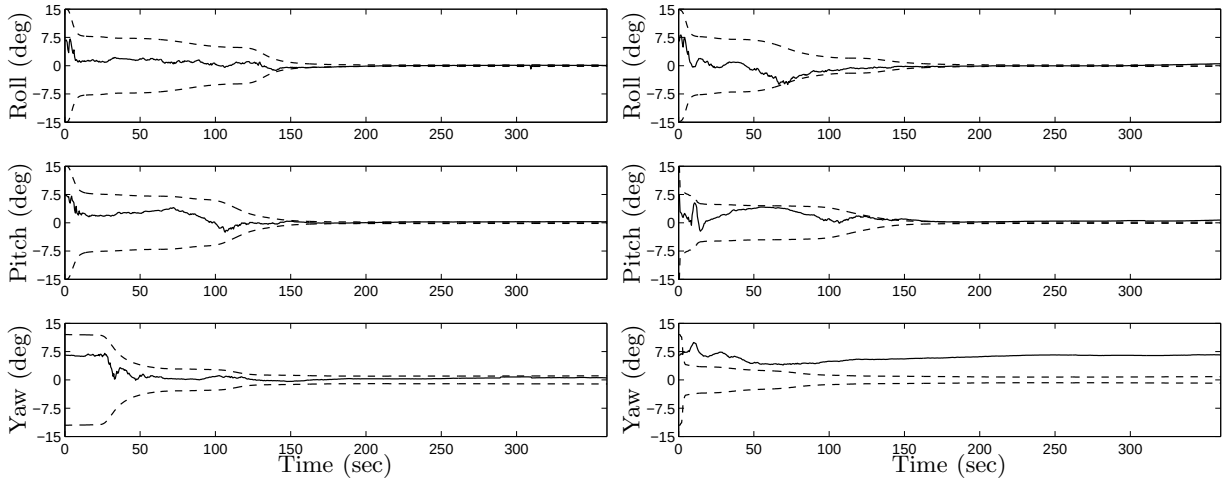

(a) 15-State EKF Attitude Errors and 3σ Bounds

(b) 17 State EKF Attitude Errors and 3σ Bounds

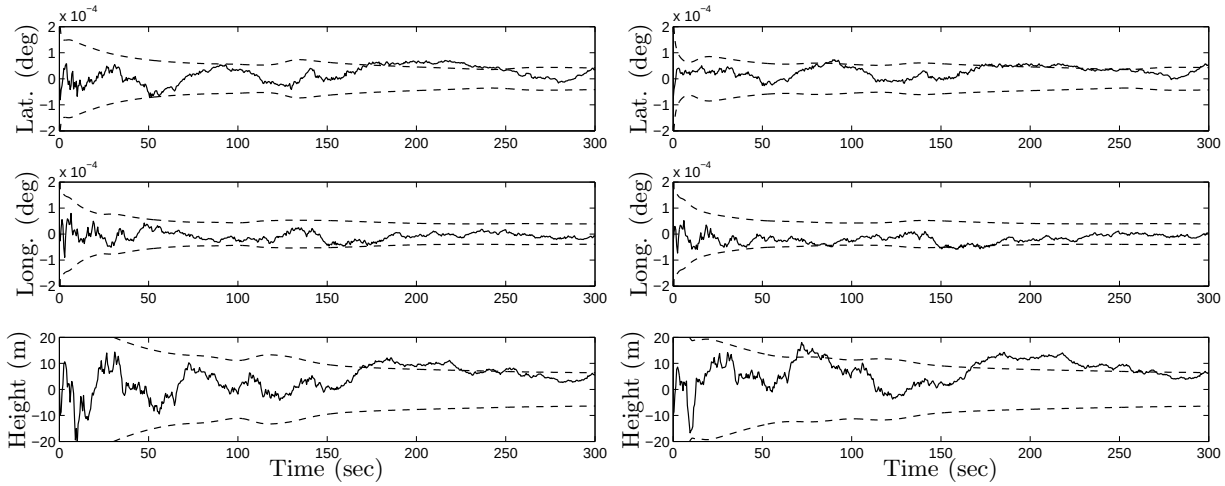

(c) 15-State EKF Position Errors and 3σ Bounds

(d) 17-State EKF Position Errors and 3σ Bounds

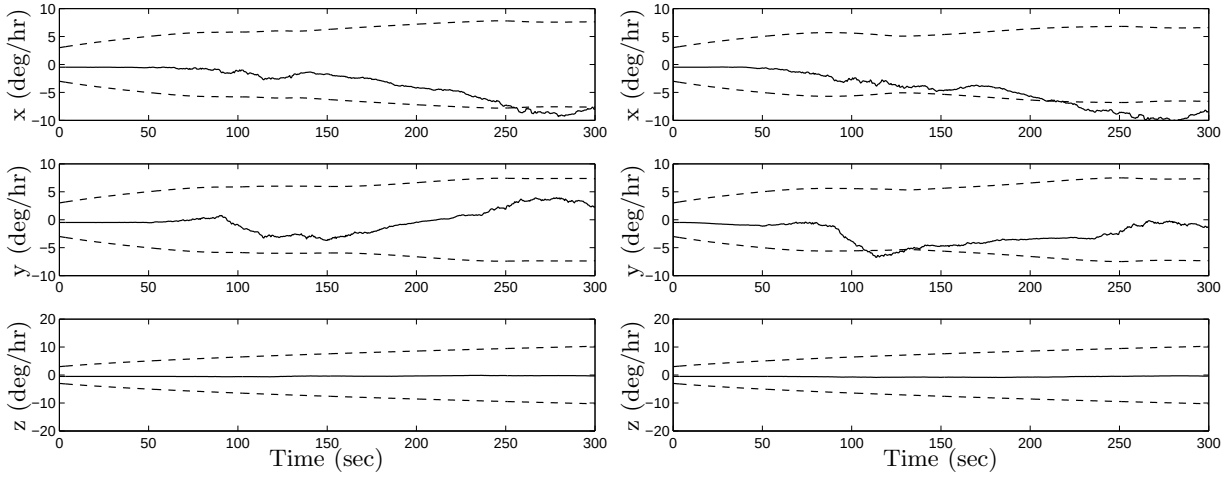

(e) 15-State EKF Gyro-Bias Errors and 3σ Bounds

(f) 17-State EKF Gyro-Bias Errors and 3σ Bounds

Figure 2. EKF Results for Added Wheel Speed Sensor

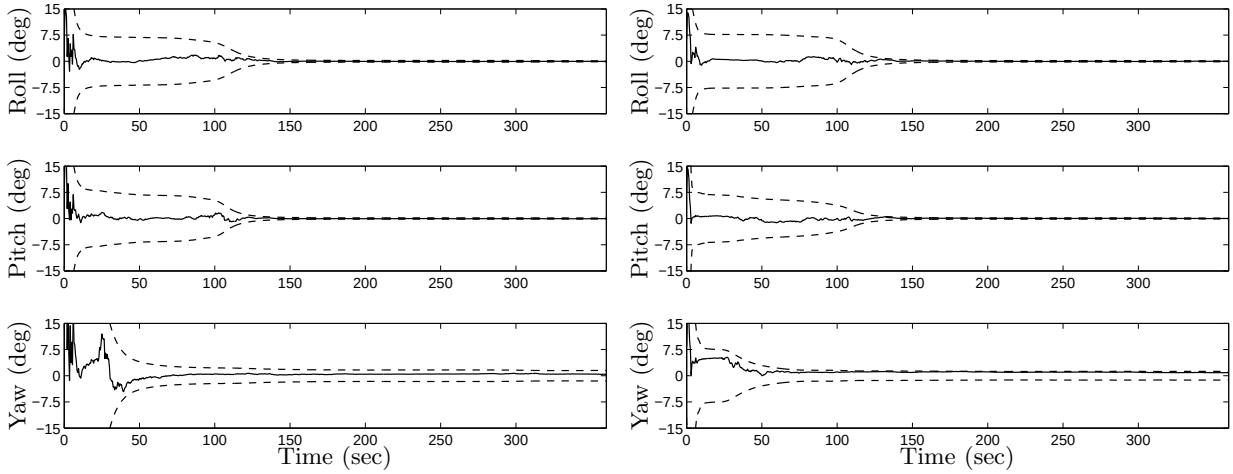

(a) 15-State UF Attitude Errors and 3σ Bounds

(b) 17-State UF Attitude Errors and 3σ Bounds

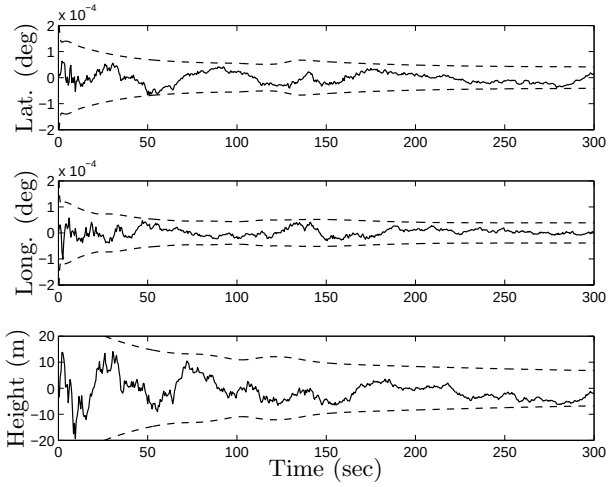

(c) 15-State UF Position Errors and 3σ Bounds

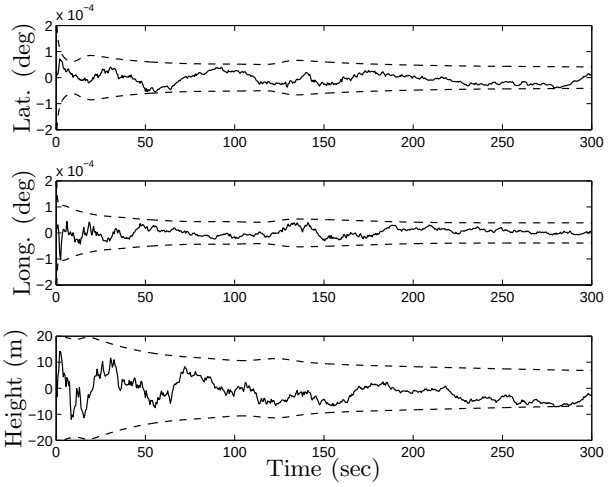

(d) 17-State UF Position Errors and 3σ Bounds

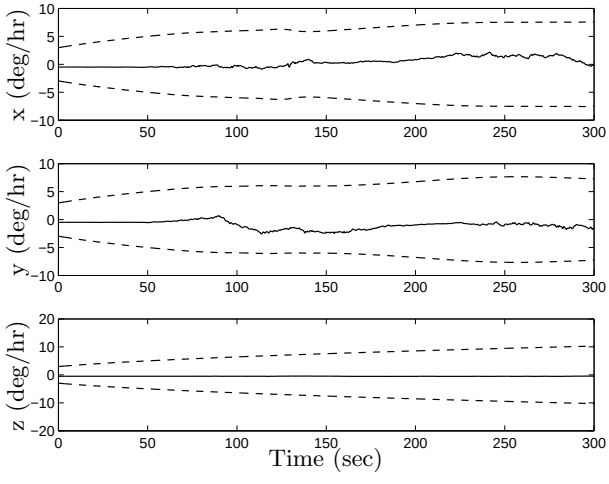

(e) 15-State UF Gyro-Bias Errors and 3σ Bounds

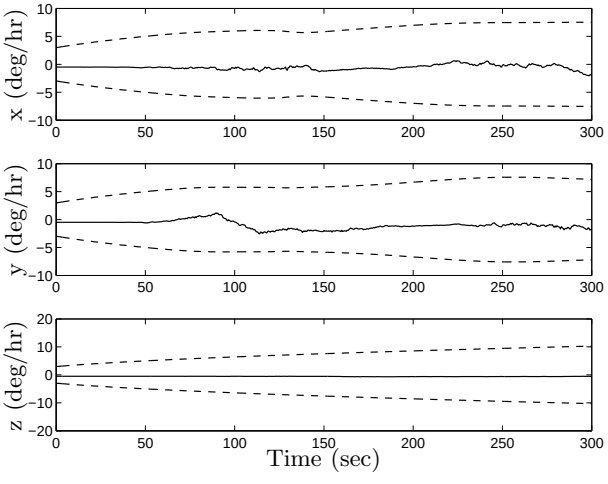

(f) 17-State UF Gyro-Bias Errors and 3σ Bounds

Figure 3. UF Results for Added Wheel Speed Sensor

Aerospace and Electronic Systems, Vol. 42, No. 2, 2006, pp. 750–756.

[7]Hay, C., "Turn, Turn, Turn Wheel-Speed Dead Reckoning for Vehicle Navigation," *GPS world*, Vol. 16, No. 10, 2005, pp. 37–42.

[8]Kubo, Y., Kindo, T., Ito, A., and Sugimoto, S., "DGPS/INS/Wheel Sensor Integration for High Accuracy Land-Vehicle Positioning," *Proceedings of the National Technical Meeting of the Institute of Navigation (ION)*, 1999, pp. 555–564.

[9]Gao, J., Petovello, M. G., and Cannon, M. E., "Development of Precise GPS/INS/Wheel Speed Sensor/Yaw Rate Sensor Integrated Vehicular Positioning System," *Proceedings of the National Technical Meeting of the Institute of Navigation (ION)*, Vol. 2, pp. 780–792.

[10]Saraf, S. and Tomizuka, M., "Slip Angle Estimation for Vehicles on Automated Highways," *Proceedings of the American Control Conference*, Vol. 3, 1997, pp. 1588–1592.

[11]Carlson, C. R., Gerdes, J. C., and Powell, J. D., "Practical Position and Yaw Rate Estimation with GPS and Differential Wheelspeeds," *Proceedings of AVEC 6th International Symposium*, Japan, 2002.

[12]Farrell, J., Barth, M., Galijan, R., and Sinko, J., "GPS/INS Based Lateral and Longitudinal Control Demonstration: Final Report," California PATH Research Report, University at California, Berkeley, CA, UCB-ITS-PRR-98-28, 1998.

[13]Julier, S., Uhlmann, J., and Durrant-Whyte, H. F., "A New Method for the Nonlinear Transformation of Means and Covariances in Filters and Estimators," *IEEE Transactions on Automatic Control*, Vol. 45, No. 3, 2000, pp. 477–482.

[14]Meeus, J., *Astronomical Algorithms*, Willman-Bell, Inc., Richmond, VA, 2nd ed., 1999.

[15]Decker, B., "World Geodetic System 1984," Defence Mapping Agency, Aerospace Center, St. Louis, MO, ADA167570, 1986.

[16]Zhu, J., "Conversion of Earth-Centered Earth-Fixed Coordinates to Geodetic Coordinates," *IEEE Transactions on Aerospace and Electronic Systems*, Vol. 30, No. 3, 1994, pp. 957–961.

[17]Shuster, M., "Survey of Attitude Representations," *Journal of the Astronautical Sciences*, Vol. 41, 1993, pp. 439–517.

[18]Lefferts, E. J., Markley, F. L., and Shuster, M. D., "Kalman Filtering for Spacecraft Attitude Estimation," *Journal of Guidance, Control, and Dynamics*, Vol. 5, No. 5, Sept.-Oct. 1982, pp. 417–429.

[19]Moler, C. and Van Loan, C., "Nineteen Dubious Ways to Compute the Exponential of a Matrix, Twenty-Five Years Later," *SIAM review*, Vol. 45, No. 1, 2003, pp. 3–49.

[20]Wan, E. A. and Van Der Merwe, R., "The Unscented Kalman Filter," *Kalman filtering and neural networks*, 2001, pp. 221–280.

[21]Bar-Shalom, Y. and Fortmann, T. E., *Tracking and Data Association*, Academic Press, Boston, MA, 1988.

[22]Bartels, R. H. and Stewart, G. W., "Solution of the Matrix Equation AX+ XB= C [F4]," *Communications of the ACM*, Vol. 15, No. 9, 1972, pp. 820–826.

[23]Crassidis, J. L. and Markley, F. L., "Unscented Filtering for Spacecraft Attitude Estimation," *Journal of Guidance Control and Dynamics*, Vol. 26, No. 4, 2003, pp. 536–542.

[24]Markley, F. L., "Attitude Error Representations for Kalman Filtering," *Journal of Guidance Control and Dynamics*, Vol. 26, No. 2, 2003, pp. 311–317.